



An application of Boussinesq modeling to Hurricane wave overtopping and inundation

Patrick J. Lynett^{a,*}, Jeffrey A. Melby^b, Dae-Hong Kim^a

^a Zachry Department of Civil Engineering, Texas A&M University, College Station, TX 77843, USA

^b US Army Engineer Research and Development Center, 3909 Halls Ferry Rd, Vicksburg, MS 39180, USA

ARTICLE INFO

Article history:

Received 31 October 2008

Accepted 28 August 2009

Available online 11 September 2009

Keywords:

Hurricane

Katrina

Overtopping

Numerical modeling

Boussinesq

ABSTRACT

Wave and combined wave-and-surge overtopping was significant across a large portion of the hurricane protection system of New Orleans during Hurricane Katrina. In particular, along the east-facing levees of the Mississippi River-Gulf Outlet (MRGO), the overtopping caused numerous levee breaches. This paper will focus on the MRGO levees, and will attempt to recreate the hydrodynamic conditions during Katrina to provide an estimate of the experienced overtopping rates. Due to the irregular beach profiles leading up to the levees and the general hydrodynamic complexity of the overtopping in this area, a Boussinesq wave model is employed. This model is shown to be accurate for the prediction of waves shoaling and breaking over irregular beach profiles, as well as for the overtopping of levees. With surge levels provided by ADCIRC and nearshore wave heights by STWAVE, the Boussinesq model is used to predict conditions at the MRGO levees for 10 h near the peak of Katrina. The peak simulated overtopping rates correlate well with expected levee damage thresholds and observations of damage in the levee system. Finally, the predicted overtopping rates are utilized to estimate a volumetric flooding rate as a function of time for the entire 20 km stretch of east-facing MRGO levees.

© 2009 Elsevier Ltd. All rights reserved.

1. Introduction

On August 29, 2005 Hurricane Katrina made landfall along the northern Gulf of Mexico coast. Among widespread destruction caused by the Hurricane was significant overtopping-related scour and breaching of the Mississippi River Gulf Outlet (MRGO), a man-made channel to the east of the New Orleans metropolitan area. Damage was severe along this 20 km stretch of primarily earthen levees, with crest elevations scoured down in excess of 3 m in numerous locations. The *Interagency Performance Evaluation Team (IPET)* (2006) was tasked with documenting the storm conditions in this area, as well as providing probable causes for the observed damage; the levee damage along the MRGO was caused by either wave overtopping or combined wave-and-surge overtopping (*ASCE Hurricane Katrina External Review Panel, 2007*).

Estimation of levee overtopping rates has traditionally made use of empirical relations based on many experimental datasets. While these relations initially focused on the simple, smooth-sloped, trapezoidal levee, modifications have been made to include complexities such as surface roughness, wave directionality, and bermed profiles (e.g. *van der Meer, 2002*). The most current tools, such as those arising from the *Eurotop* (*Pullen et al., 2007*) efforts, are able to accommodate from general to complex

geometries, and are also able to provide uncertainties in the estimates. The relative computational simplicity of the empirical guidance makes them very useful for probabilistic design (*Van Ledden et al., 2007*), however, these equations are only valid for the parameter ranges used in their empirical curve fit. As will be discussed in this paper, during Hurricane Katrina at the MRGO levees, the established engineering guidance is not applicable for a significant portion of the storm, and an alternative approach must be used.

One approach which permits a high degree of hydrodynamic and bathymetric flexibility is the use of time-dependent numerical models. Here, the focus is on phase-resolving models, such as those based on the Boussinesq equations. While such models do indeed offer the user an ability to simulate arbitrary waves and structure profiles, they also include approximations of important physics, such as for the interaction of fluid with a rough bottom. These approximations can lead to a level of uncertainty that is difficult to quantify; the need to use a numerical model for a situation with little or no measured data presents a validation paradox. However, with continued calibration of these models with available data, confidence can be developed and, at least initially, numerical models can be used to supplement empirical engineering guidance.

A wide range of numerical models have been developed to simulate overtopping processes. Initial studies employed the non-dissipative shallow water wave equation model (e.g. *Kobayashi and Wurjanto, 1989*). These approaches cannot capture the frequency dispersion physics of nearshore wind waves, but, at

* Corresponding author.

E-mail address: plynett@civil.tamu.edu (P.J. Lynett).

the time, were one of a few model choices that were computationally practical. More recently, researchers have developed very robust and accurate solvers for runup and overtopping with the shallow water equations (Hu et al., 2000; Hubbard and Dodd, 2002), facilitating their use for engineering studies. There are few overtopping studies using the Boussinesq equation model, an example is Stansby and Feng (2004). One possible reason for this is that the Boussinesq model, with its attractive ability to simulate dispersive wind waves, generally requires a complex numerical scheme for accuracy, a numerical scheme that does not readily lend itself to capturing the complex flow patterns (e.g. flow re-entrance on the leeside of a levee) common with overtopping. These complexities are, generally, handled in a more physically satisfactory manner in models that make no assumptions of the vertical flow structure. Navier–Stokes based approaches (e.g. Liu et al., 1999; Li et al., 2004; Shao et al., 2006; Ingram et al., 2009) have shown to be accurate in predicting both the average overtopping rates as well as the relatively small scale dynamics that govern processes such as scour and impact pressures. However, Navier–Stokes approaches are still very computationally expensive to run, although this is changing, and their engineering use is generally restricted to a small number of specific wave and structure configurations.

To compare with the numerical models, and more importantly to develop the much relied upon empirical overtopping guidance, there exists a wealth of experimental data. Though old, the regular wave data of Saville (1955) is perhaps the mostly commonly found dataset in numerical validations (e.g. Kobayashi and Wurjanto, 1989; Dodd, 1998; Hu et al., 2000). This, and a large body of much more recent data for a wider range of hydrodynamic and levee configurations (see for example De Rouck et al., 2009 and other papers in same special CLASH issue of Coastal Engineering) has been integrated into the empirical equations that most commonly guide engineering design in current practice. While the empirical methods will be a reasonable approach for the large majority of possible levee configurations, there will always be odd geometries or hydrodynamic conditions, where proper application of such methods is unclear. In these cases, the use of a validated numerical model, either on its own or coupled with an empirical approach, represents an attractive way to handle such complexity. It will be one of the main goals of this paper to develop a numerical model application procedure for an area with very uncommon beach profiles.

The approach developed in this paper is centered on the use of a Boussinesq wave model to provide detailed and accurate predictions of wave runup and overtopping of earthen levees. Validation of the wave model for interaction with levees will first be demonstrated. This validation will use both small and large scale experimental data for runup and overtopping. With confidence that the Boussinesq model can accurately capture wave shoaling, breaking, runup, and overtopping of irregular bathymetry/topography, it will be applied at four different transects along the east-facing MRGO levees. The transects examined here are earthen levees, without sheet-piles or flood gates. Predictions of overtopping rates and levee crest velocities will be correlated, in a qualitative manner, to the observed level of damage. Finally, the Boussinesq model output will be used to characterize the likely overtopping rate along the entire 20 km-long section of levees, and integrated overtopping rates will be presented.

2. Review of MRGO damage from pre- and post-Katrina lidar surveys

The levee system along the MRGO consisted, pre-Katrina, of a complex system of earthen levees, sheet-piles, and flood gates. Crest elevations varied from 5.5 to < 4 m along the 20 km length of the east-facing levees. These, and all elevations presented in

this paper, are referenced to NAVD88 2004.65. Wave heights and water levels varied weakly along the length, with the northern most levees experiencing the highest surge and waves. From the IPET study, maximum surge elevations during Katrina in this area were approximately 5.5 m according to post-Katrina survey analysis and ADCIRC simulations, and maximum significant wave heights were near 1.75 m, with peak periods of 13–14 s, according to STWAVE results. The peak wave conditions occurred about 2 h after the peak surge condition.

Levee damage, in terms of breaches and scour, was widespread and extensive along the MRGO levees. Before- and after-Katrina lidar surveys of four different segments are given in Figs. 1–4. These images show a spatially irregular damage pattern consistent with breaching, where post-Katrina levee elevations regularly change 2 m across a horizontal distance of tens of meters. These four segments are shown in detail here, as they will be the focus of the detailed hydrodynamics modeling presented in Section 7.

To further elucidate the magnitude of scour, Fig. 5 provides the change in levee crest elevation for the entire 20 km of the east facing levees. The northern third of the segment, from 0 to 7 km in Fig. 5, experienced a fairly constant level of scour on the order of 2 m, although at the far northern end, where the levee crest elevations are highest, there is only minimal erosion. Along the middle third of the segment, the scour is irregular and is largely a function of whether the levee consisted of an earthen mound, sheet pile, or flood gate. Finally, in the last, southern-most third of the segment, from 14 to 20 km in Fig. 5, the damage is relatively low to near zero. Also in this figure are shown the four locations to be examined during the Boussinesq model analysis, all of which are earthen levees. The first three points experienced very similar hydrodynamic conditions, but have different design profiles, different crest elevations, and experienced different damage levels. The fourth point represents conditions on the opposite end of the levee system, where the damage was relatively light. It is worthwhile to note that, when the MRGO Boussinesq simulations described later in this paper were originally performed during the IPET study, the detailed damage information given in this section was not yet known. In this sense, the inferred damaged level from the Boussinesq model results represents a blind comparison with the lidar data.

3. Current engineering guidance for overtopping calculations

3.1. Wave overtopping of a levee

When the still water level is below the levee crest but the waves are sufficiently large, volumetric overtopping of the levee due to waves only can occur. The CEM (2002), TAW (van der Meer, 2002), and EurOtop (Pullen et al., 2007) manuals provide wave overtopping formulae for bermed and straight impermeable levee slopes based on a wide range of small- and large-scale laboratory experimental data. The equations are similar. Therefore, only the TAW/EurOtop relations will be given as they are more recent. The average volume rate of irregular wave overtopping per unit length of structure q is given by

$$\frac{q}{\sqrt{gH_{mo}^3}} = \frac{0.067}{\sqrt{\tan \alpha}} \gamma_b \zeta_{om-1.0} \exp\left(-4.75 \frac{R_c}{H_{mo}} \frac{1}{\zeta_{om-1.0} \gamma_b \gamma_f \gamma_\beta \gamma_v}\right) \quad (1)$$

and

$$\frac{q}{\sqrt{gH_{mo}^3}} \leq 0.2 \exp\left(-2.6 \frac{R_c}{H_{mo}} \frac{1}{\gamma_f \gamma_\beta}\right) \quad (2)$$

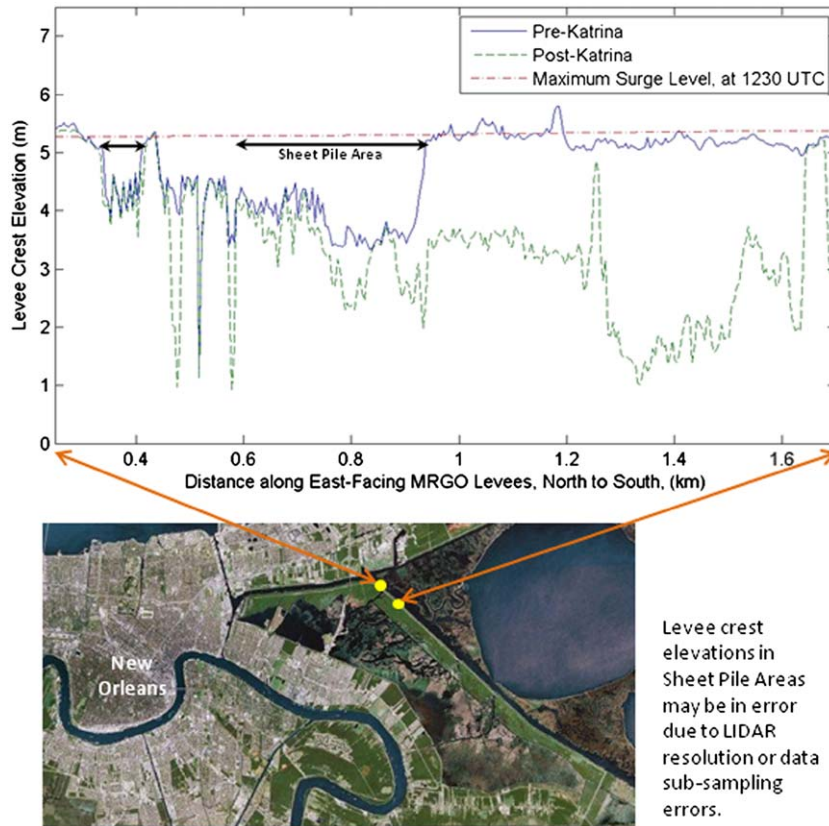


Fig. 1. Before and after Hurricane Katrina lidar survey data along the northern-most section of the MRGO levee system.

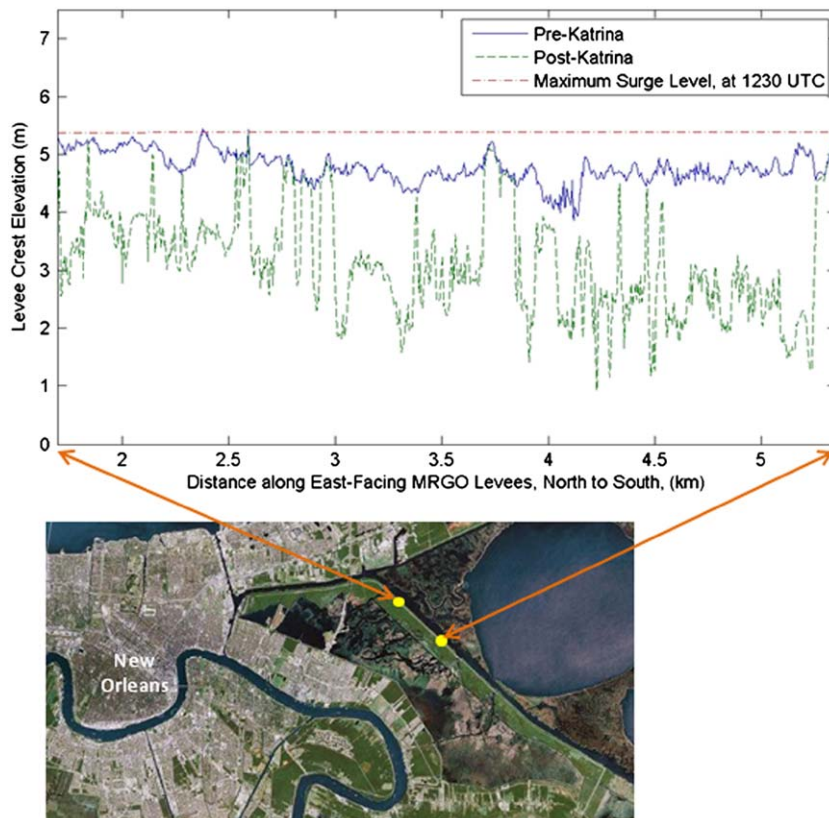


Fig. 2. Before and after Hurricane Katrina lidar survey data along the northern-middle section of the MRGO levee system.

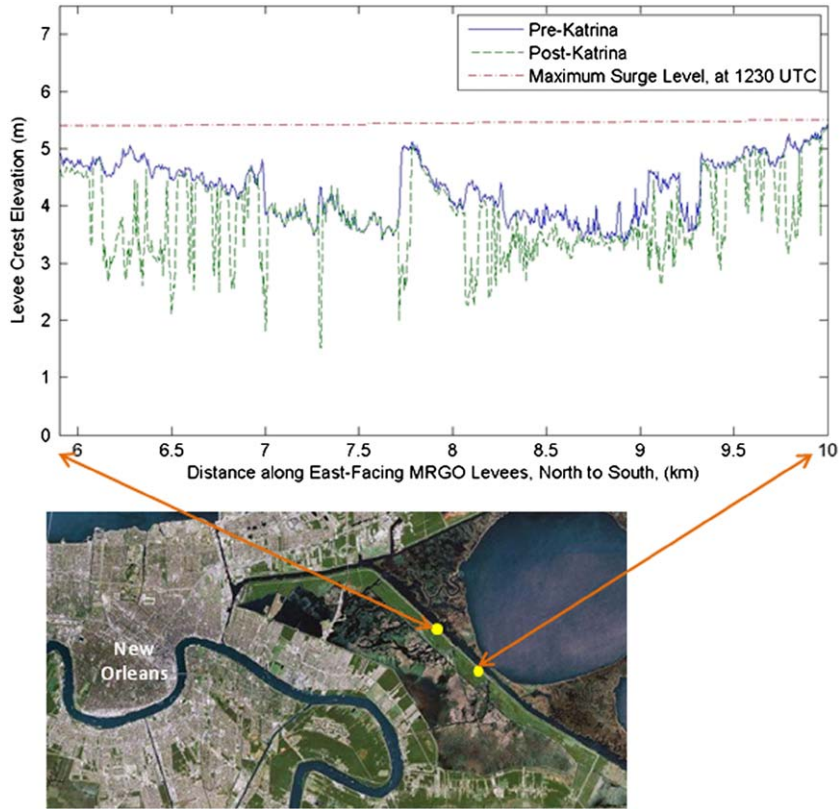


Fig. 3. Before and after Hurricane Katrina lidar survey data along the southern-middle section of the MRGO levee system.

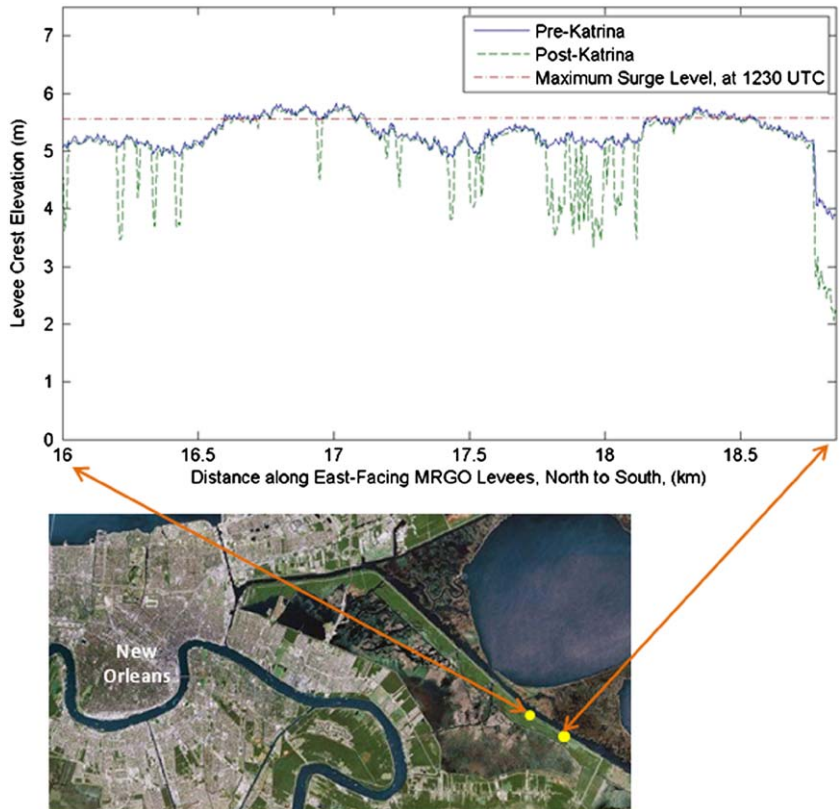


Fig. 4. Before and after Hurricane Katrina lidar survey data along the southern-most section of the MRGO levee system.

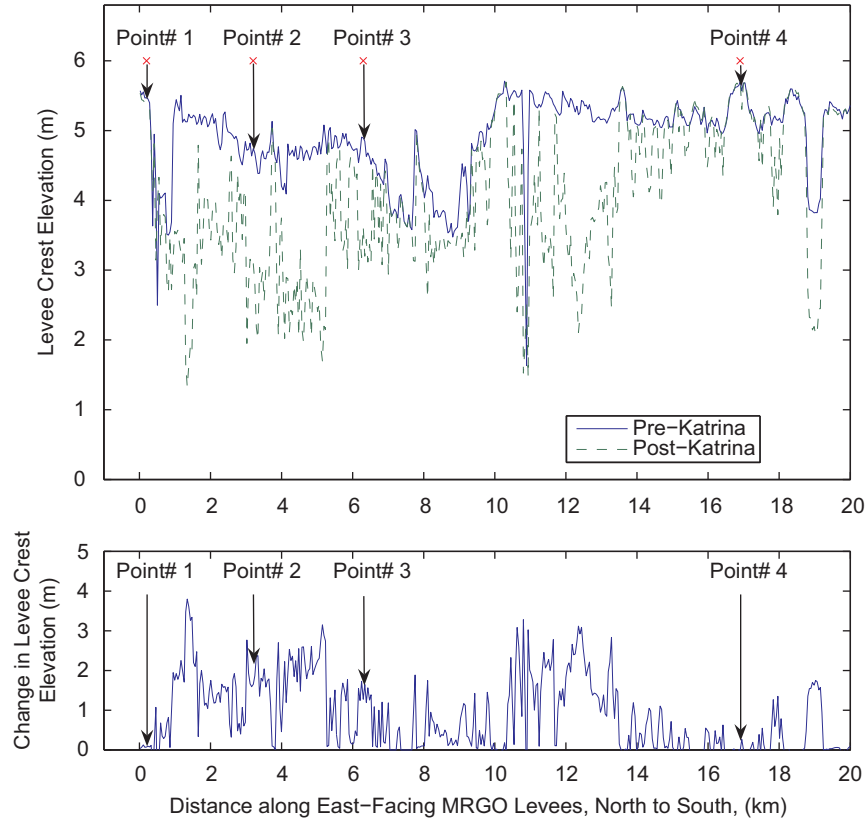


Fig. 5. Before and after Hurricane Katrina levee crest elevations, taken from the lidar data, along the entire length of the east-facing MRGO levee system. In the lower subplot, the change in elevation is shown. The four “points” indicate the locations at which the Boussinesq model is used to simulate storm conditions.

where R_c is the structure crest height above the still water level, g is acceleration of gravity, $\tan \alpha$ is the seaside slope of the levee, and the various other parameters will be described in this section. Note that the above overtopping equations are dimensionally consistent. The significant wave height is defined as $H_{m0} = 4\sqrt{m_0}$ where $m_0 =$ zeroth moment of the wave energy density spectrum. The Iribarren parameter, ξ_{om-1} , is defined as

$$\xi_{om-1} = \frac{\tan \alpha}{\sqrt{s_{om-1}}}, \quad s_{om-1} = \frac{H_{m0}}{L_{om-1}}, \quad L_{om-1} = \frac{gT_{m-1,0}^2}{2\pi} \quad (3)$$

The spectral period, $T_{m-1,0} = m_{-1}/m_0$, where $m_{-1} =$ first negative moment of the wave energy density spectrum, is used in Eq. (3). Reduction factors included are $\gamma_f =$ influence of surface roughness, $\gamma_b =$ influence of berm, $\gamma_v =$ influence of wall on slope, and $\gamma_\beta =$ influence of angle of wave incidence. The CEM (Section VI-5-2) provides a summary of the studies conducted to generate coefficients for Eq. (1) for varied structure slopes, wave conditions, and roughness characteristics. Some typical values for coefficients are $\gamma_v = 1$ for no wall, $\gamma_v = 0.65$ for a wall at the top of the seaward slope, and $\gamma_\beta = 1$ for normally incident waves. The influence of oblique waves is negligible for long-crested waves between normal and 30° .

TAW suggests that Eqs. (1) and (2) are valid for slopes 1V:1H to 1V:8H and recommends $0.5 < \xi_{om-1} < 10$ with the range 8–10 being less accurate. In addition, the valid parameter range for Eqs. (1) and (2) is

$$0.3 < \frac{R_c \sqrt{s_{op}}}{H_s \tan \alpha \gamma_f \gamma_b \gamma_v \gamma_\beta} < 2 \quad (4)$$

According to CEM Table VI-5-6, damage to grass-covered levees will begin to occur if $q = 0.001\text{--}0.01 \text{ m}^3/\text{s/m}$ ($q = 1\text{--}101 \text{ s/m}$).

The empirical equations above were based on best central fits to mostly small-scale laboratory data with a small amount of larger

scale data. The equations are limited to the range of the limited test conditions. Much progress has been made during recent European overtopping studies as additional data and analysis have become available. The result has been an evolution of the empirical coefficients for these equations. However, this illustrates the limitations of equations based nearly entirely on best fits to limited data. Despite very talented and experienced researchers, data alone do not support conclusive guidance for these complex physical processes. Additionally, the erosion limit states discussed above are based on extremely limited field tests and have not yet been validated. Finally, because virtually all of the experimental data is for wave overtopping without the presence of steady flow, or for steady flow with no overtopping, at the time this study was done, there was no empirical guidance for the combined overtopping and steady-flow conditions on the MRGO levee during Hurricane Katrina. Since then Hughes and Nadal (2009) have conducted a generalized study of combined overtopping and steady flow.

3.2. Steady-flow overtopping of levee

When the water level is higher than the crest of the levee, steady flow will occur. This physical process was described clearly by Powledge et al. (1989). Flow is subcritical on the seaward side of the levee and supercritical on the landward side. Flow on the seaward side will not be erosive for steady flow unless the crest materials are highly erodible. Near the landward limit of the levee crest, the flow transitions to critical and then supercritical. Materials can erode in this region depending on the flow velocity and the erodibility of the materials. The leeside crest corner is particularly susceptible to erosion if the material is erodible. Along the levee backside, the flow accelerates to fully developed supercritical and proceeds downslope until it reaches the base of

the slope or the leeside pool where a hydraulic jump develops. Erosion can occur due to high velocities on the lee side and due to turbulence under the hydraulic jump. The toe of the slope is the most common location for initiation of erosion. The erosion typically progresses upslope as a headcut develops.

Steady-flow overtopping of levees is similar to overtopping of a broad-crested weir, which is covered in hydraulics textbooks. An evaluation of the energy balance across the weir yields the relation for discharge per running length:

$$q = (2/3)^{3/2} \sqrt{g}(h_s - h_c)^{3/2} = 0.54 \sqrt{g}(h_s - h_c)^{3/2} \quad (5)$$

where h_s is the seaside water (surge) elevation, h_c is the levee crest elevation, and g is the acceleration of gravity. Note that the levee freeboard, R_c , is equal to $h_c - h_s$. Eq. (5) is dimensionally consistent and is commonly applied to levee overtopping discharge. Grass on levees produces some reduction in overtopping flow; however, this reduction is often neglected for conservative design.

3.3. Combined wave and steady-flow overtopping

There is little empirical design guidance for the condition when the water level is above the crest and there is both steady flow and significant wave overtopping. It is expected that this

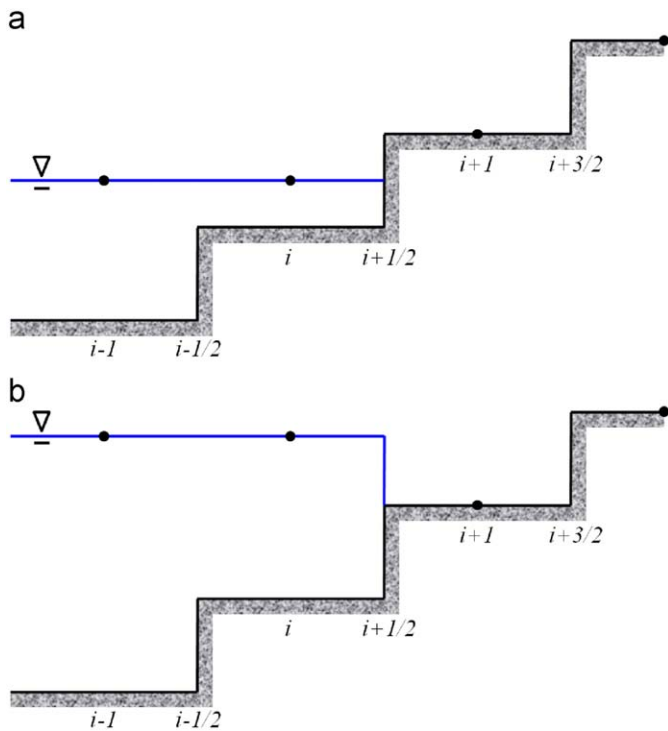


Fig. 6. Schematic diagram of moving boundary.

condition would be highly erosive, particularly for shallow water on the crest. Equations were proposed by Schüttrump et al. (2001) and refined in the Eurotop manual for zero-freeboard overtopping. The Eurotop manual suggested that zero-freeboard wave and steady-flow overtopping equations be linearly superimposed to compute combined overtopping. Recently, Reeve et al. (2008) and Hughes and Nadal (2009) have performed numerical and physical studies, respectively, of combined wave and surge overtopping. These provide a new set of data and curve fits for situations with small positive to small negative freeboard, and corresponding sets of empirical guidance.

4. Detailed hydrodynamic modeling

In this section, the Boussinesq modeling approach will be introduced. The governing equations, numerical scheme, and moving boundary approach will be presented.

4.1. Boussinesq equations

The conservative form of weakly dispersive and fully nonlinear depth-integrated form of Boussinesq equations in one-horizontal-dimension are expressed as (e.g. Kim et al., 2009)

$$\frac{\partial H}{\partial t} + \frac{\partial H U_x}{\partial x} + D^c = 0 \quad (6)$$

$$\frac{\partial H U_x}{\partial t} + \frac{\partial H U_x^2}{\partial x} + g H \frac{\partial \zeta}{\partial x} + g H D^x + U_x D^c - R_b^x = 0 \quad (7)$$

where $H = \zeta + h$ is a total water depth, ζ is water surface elevation, h is water depth. U_x is velocity at water depth z_x in the x direction. The D^c and D^x are the higher order terms that include the bottom turbulence and dispersive properties. To approximate the bottom stress, a quadratic friction equation is used:

$$\tau_b^x = \frac{C_f u \sqrt{u^2}}{\rho} \quad (8)$$

where τ_b^x is the bottom stresses in the x direction, ρ is the fluid density, and u is the depth averaged velocity in the x direction. The roughness coefficient $C_f = f/4$ (Chen and Jirka, 1995) and f is estimated with a given roughness height, k_s , using the Moody diagram, which here is calculated by the explicit formula given by Haaland (1983). The R_b^x term is the wave breaking related dissipation term proposed by Lynett (2006). More detailed descriptions of each term can be found in Kim et al. (2009) and Lynett (2006).

4.2. Numerical scheme

Complete details of the numerical solution scheme can be found in Kim et al. (2008), and a brief overview is given here. A third-order Adams–Bashforth predictor and the fourth-order Adams–Moulton corrector scheme are used for the time

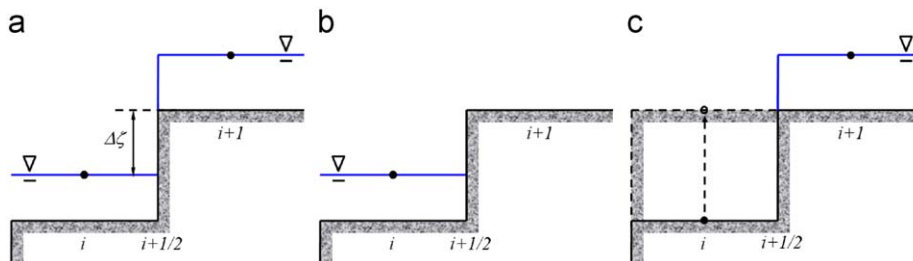


Fig. 7. Schematic diagram of moving boundary.

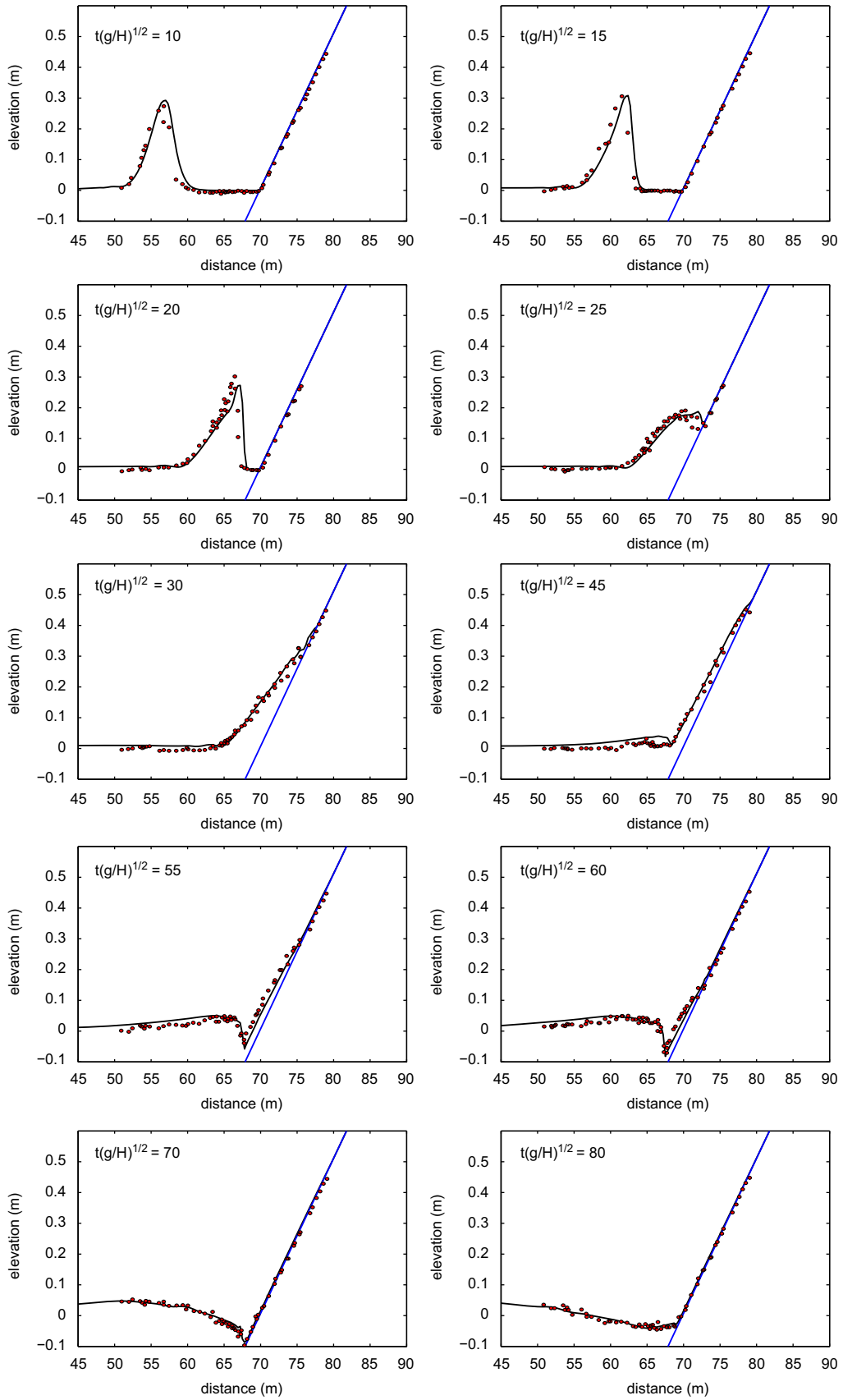


Fig. 8. Water surface profiles for runup and rundown process. Breaking case ($\epsilon = 0.28$). Line: numerical data and dot: experimental data.

integration. The spatial representation of the numerical grid is a Finite Volume scheme. For the calculation of leading-order (shallow water) terms in the governing equations, a fourth-order compact MUSCL TVD (monotone upstream-centered scheme for conservation laws–total variation diminishing) scheme (Yamamoto and Daiguji, 1993) is used. For the second-order (dispersive) terms, a cell averaged finite volume method is implemented. Spatial and temporal resolution of the numerical results will be expressed through the grid spacing, Δx and the Courant number, C_r . The scheme has been shown to be highly stable and accurate, and capable of capturing shock fronts without numerical dispersion errors.

4.3. Moving boundary scheme

In this paper, a very simple physical condition is proposed for the moving boundary scheme. Essentially it follows the approach proposed by Liu et al. (1995) except for one condition described below. As shown in Fig. 6(a), if the water surface level at i is lower than the level of the dry bed at $i+1$, then the variables at $i+1/2$ are evaluated by assuming that there is a wall at $i+1$. Here the i index represents a spatial cell location. On the other hand, if the water surface level at i is higher than the level of the dry bed at $i+1$, as in Fig. 6(b), the water is supposed to flow into the cell $i+1$. Note that this moving boundary scheme assumes discontinuous bottom topography, so the modified surface gradient method that can be applied on discontinuous bottom topography should be used (Kim et al., 2008). Without employing such a method, non-physical oscillations can be created at the boundary of the wet and dry bed.

A physical constraint is added to the scheme, determined largely from experience in using it. Similar to other moving boundary schemes (e.g. Lynett et al., 2002), some minimum allowable total water depth must be chosen. When the total water depth is very small, the computed velocity can become very large, often due to a poor representation of bottom friction for these cases, causing the required time step for stability to plummet. Here, if the total water depth is $< \varepsilon_h$, then the computed velocity is set to zero. For idealized flow simulations on a simple bottom, ε_h can be $< 1 \times 10^{-6}$ m or less. However, for complex flow simulations, $\varepsilon_h = 1 \sim 2 \times 10^{-4}$ m is recommended.

However, for a particular situation shown in Fig. 7, non-physical and unstable computations can occur even if the above described moving boundary scheme is implemented correctly. In Fig. 7(a), physically, the water at cell i must not affect the flow at $i+1$, but the water at $i+1$ can affect the flow at i . Therefore, in order to reflect this particular situation in the numerical model, the flux at $i+1/2$ is divided into two parts following the Fig. 7(b) and (c). The fluxes for each interface side are calculated independently, and then combined. In detail, in one-dimensional space,

- (1) Divide the case (a) into (b) and (c) as in Fig. 7.
- (2) For the case of (b), compute the fluxes for cell i as if there was a vertical wall at $i+1/2$.
- (3) For the case of (c), assume the bottom level of cell i to be the same with the bottom level of cell $i+1$, and compute the fluxes of the cell $i+1$ (as if on flat bed).
- (4) Sum the computed fluxes at $i+1/2$ from case (b) and (c), and use that total flux in the application of the governing equations for cells i and $i+1$.

With this moving boundary scheme, all equations are solved directly without extrapolations as used in Lynett et al. (2002), for example. Thus, it is anticipated that physical solutions with less

loss of mass can be obtained and overtopping of steep walls can be solved as well.

Small numerical oscillations may be still created at the shoreline where flow is particularly energetic, and is typically due to the dispersive terms, and their high-order expression. To get rid of the unwanted numerical oscillations, a combination of shallow water equations and Boussinesq equations is used. In this paper, if one or more of the three cells to the left or three cells to the right have the total water depths $< \varepsilon_h$, the shallow water equations are solved; otherwise Boussinesq equations are employed. This criterion is physically reasonable as, in shallow water, that is near the shoreline, depth-integrated flow properties can be reasonably predicted by the conventional nonlinear shallow water models.

5. Validation of Boussinesq model for wave runup and overtopping

In this section the performance of the proposed moving boundary scheme is tested. The validations are based on the comparisons to experiments with deterministic approach. Even though relatively simple waves are generated at the offshore area of modeling domains, the physical processes become complex around the levees. Therefore, under the assumption that the Boussinesq equations model can predict the behavior of runup and overtopping reasonably, it can be expected that reliable overtopping rate can be obtained if proper time series at boundary, even irregular, is given from ADCIRC and STWAVE.

Table 1

Experimental setup of the BEB sinusoidal wave overtopping.

Test no.	h (m)	h_s (m)	h_c (m)	H (m)	T (s)	s
1	0.529	0.081	0.054	0.107	1.549	3.0
2	0.529	0.081	0.107	0.107	1.549	3.0
3	0.609	0.161	0.054	0.107	1.549	3.0
4	0.609	0.161	0.107	0.107	1.549	3.0
5	0.609	0.161	0.054	0.081	1.858	3.0
6	0.529	0.081	0.054	0.107	2.616	3.0
7	0.529	0.081	0.107	0.107	2.616	3.0
8	0.529	0.081	0.161	0.107	2.616	3.0
9	0.609	0.161	0.054	0.107	2.616	3.0
10	0.609	0.161	0.107	0.107	2.616	3.0
11	0.609	0.161	0.161	0.107	2.616	3.0
12	0.529	0.081	0.054	0.081	3.634	3.0
13	0.609	0.161	0.054	0.081	3.634	3.0
14	0.609	0.161	0.107	0.081	3.634	3.0
15	0.609	0.161	0.161	0.081	3.634	3.0
16	0.609	0.161	0.215	0.081	3.634	3.0
17	0.529	0.081	0.054	0.107	2.616	1.5
18	0.529	0.081	0.161	0.107	2.616	1.5
19	0.448	0.000	0.054	0.107	2.616	1.5
20	0.448	0.000	0.107	0.107	2.616	1.5

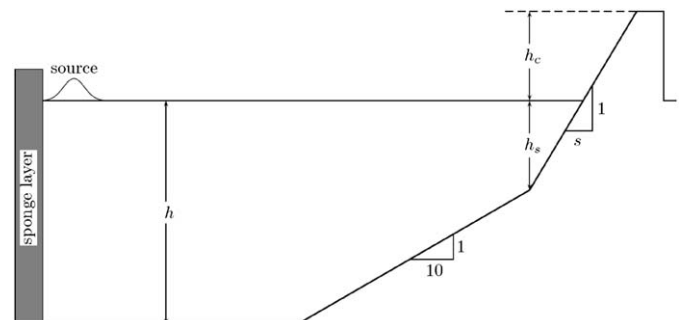


Fig. 9. Laboratory experiment setup of BEB.

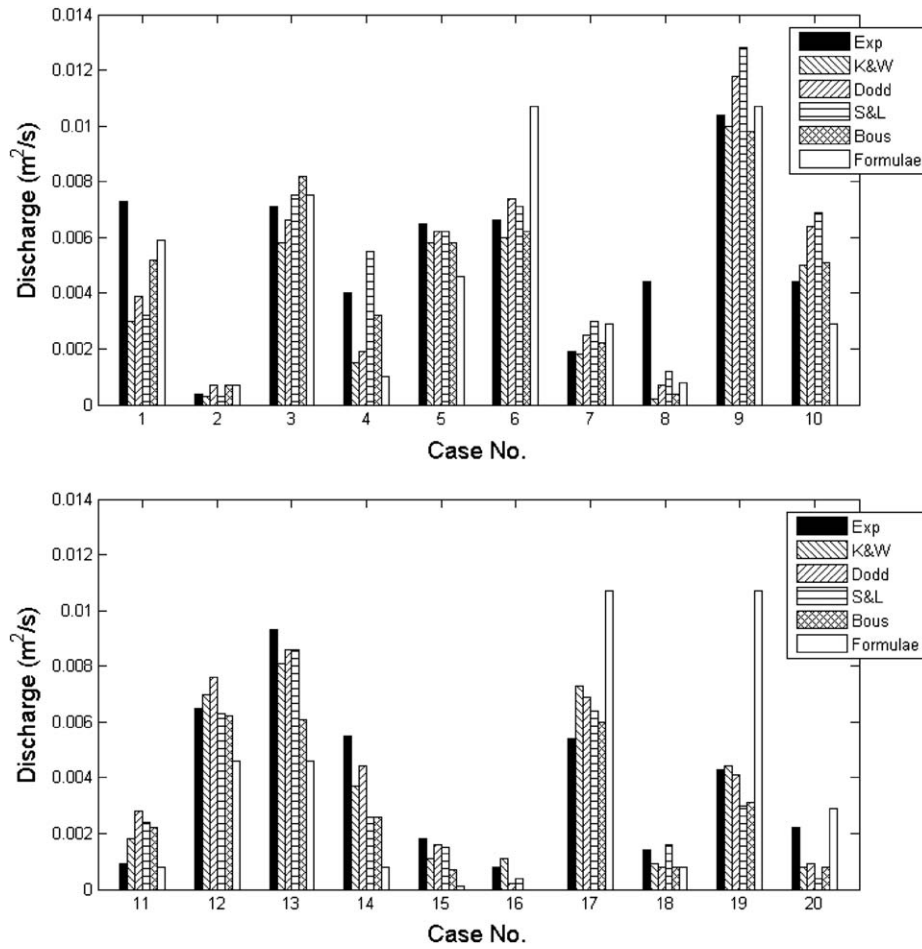


Fig. 10. Overtopping fluxes over the Saville levees. In each group of bars, from left to right: Exp: Saville (1955); K&W: Kobayashi and Wurjanto (1989); Dodd: Dodd (1998); I&L: Sitanggang and Lynett (2009); Bous: present study; and Formulae: empirical equations in Section 3.1.

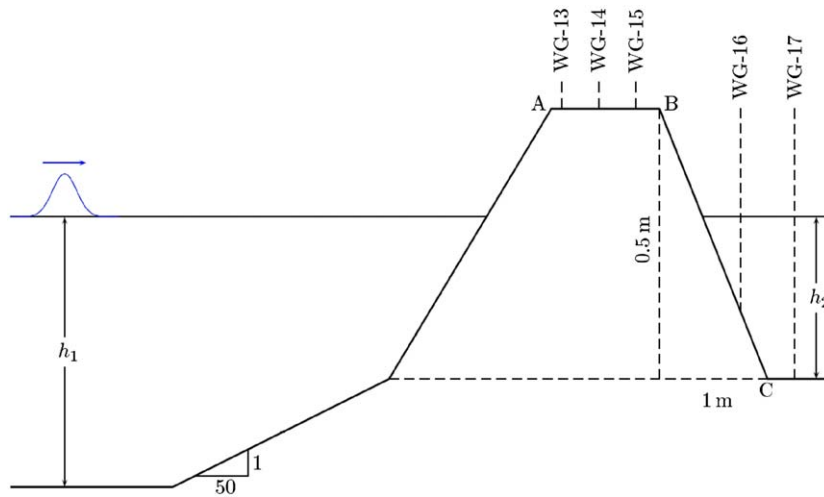


Fig. 11. Laboratory experiment setup of HR Wallingford.

Note that no modification of the bathymetry, such as smoothing/ filtering, is done for any of the computations in this paper.

5.1. Solitary wave runup and rundown

For the verification of the moving boundary scheme, one of the most commonly compared solitary wave runup and rundown

datasets, investigated experimentally by Synolakis (1987), is used. In Synolakis' experiments, the beach slope was 1:19.85 and various wave nonlinearities, ε the wave height to depth ratio, were tested. To compare with the data, a wave with $\varepsilon=0.28$ is simulated; this solitary wave breaks before reaching the shoreline. For the numerical simulations, $\Delta x=0.3$ m, $C_r=0.5$ and, for the bottom friction, $k_s=0.1$ mm. During this breaking wave runup simulation, the breaking dissipation term R_b is incorporated into

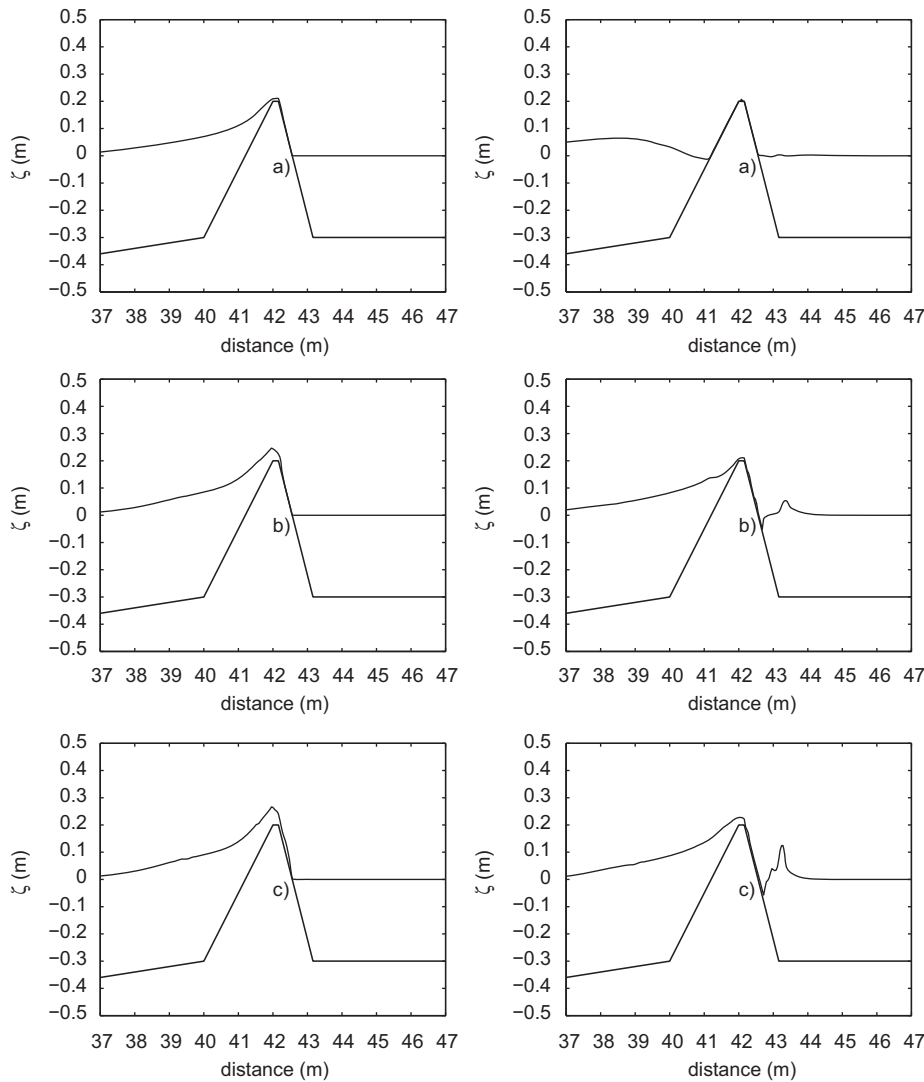


Fig. 12. Snapshot of computed water surface profiles. Wave heights: (a) 0.07 m, (b) 0.10 m, and (c) 0.12 m.

the momentum equations. The computed results are compared with the experimental data in Fig. 8. The proposed moving boundary scheme produces very good agreement and stable results for both the runup and rundown process. These comparisons provide a measure of confidence that the moving boundary scheme can reproduce well-controlled, small-scale measurements.

5.2. Overtopping of a simple levee

Here, overtopping experimental data reported in Saville (1955) are compared with computational results. The experiment was conducted by the Beach Erosion Board (BEB). The flume was made of concrete and was 36.6 m long, 1.52 m wide, and 1.52 m deep. At upstream side, a wavemaker was used for regular sinusoidal wave generation. At the downstream end of the flume, levee structures were built. A structure with slope 1:s was fronted by a fixed 1:10 sloped floor. The setup of the waves and the structures are summarized in the Table 1 and Fig. 9.

In the numerical simulations, the sinusoidal (regular) wave is generated using an internal source generator combined with the sponge layer on the upstream boundary. $\Delta x = 0.05$ m, $C_r = 0.5$, and

$k_s = 0.0006$ m are used and the overtopping fluxes are evaluated on the levee crest. The breaking dissipation terms are included in all the computations. For the comparisons, other computed results by the shallow water equation models of Kobayashi and Wurjanto (1989) and Dodd (1998), and the Reynolds averaged Navier–Stokes model by Sitanggang and Lynett (2009) are compared together in Fig. 10. Additionally, the overtopping predictions provided by the empirical guidance, using the equations given in Section 3.1, are shown. Note that, when using the empirical equations of Section 3.1, the average beach slope is used for the levee slope, all reduction coefficients are set to 1.0, and the wave heights as given in Table 1 are used directly. If one were to convert the regular wave Saville heights to an “equivalent” significant wave height by multiplying them by a factor of $\sqrt{2}$, the empirical overtopping predictions would all be considerably larger than those presented in Fig. 10. No perfect match is observed, and, for the tests nos. 8, 11, and 20, the computed results were either much smaller or larger than the measured data. Comparing the numerical results and the empirical predictions, the average agreement with the experimental trails is similar, with the numerical results yielding clearly better results for some cases (e.g. nos. 6, 12, 17, and 19) and the empirical results more accurate in others (e.g. nos. 11 and 20). In the overall sense, the present

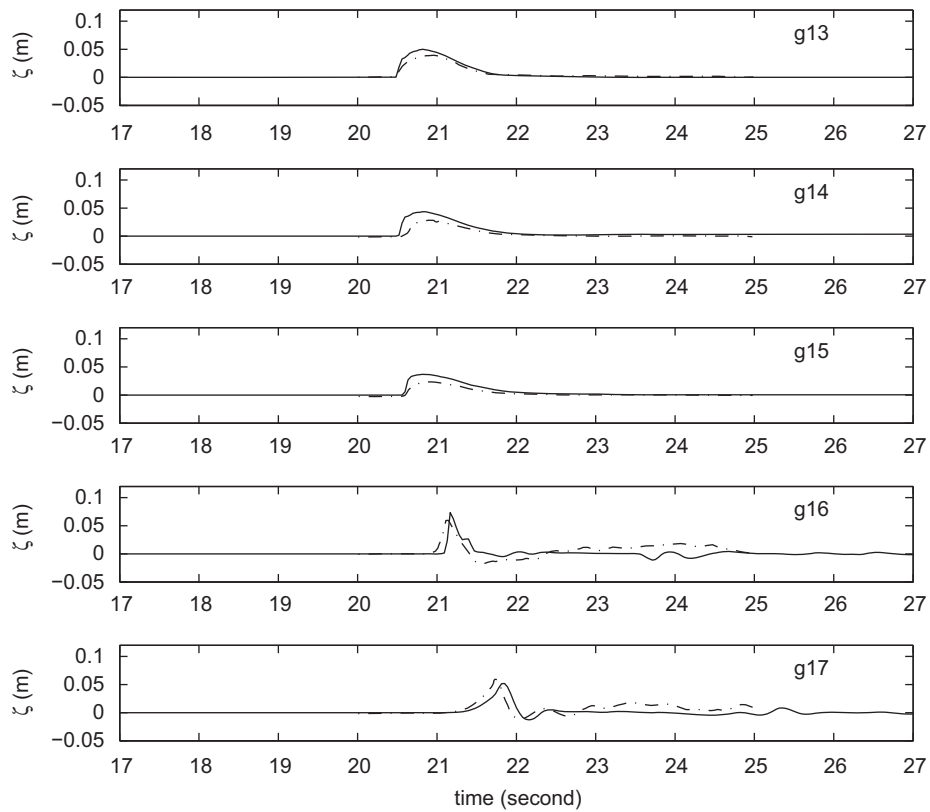


Fig. 13. Time series of the water surface elevations: wave height = 0.10 m, solid: numerical, dotted: experiment. The gage, “g”, locations follow those shown in Fig. 11.

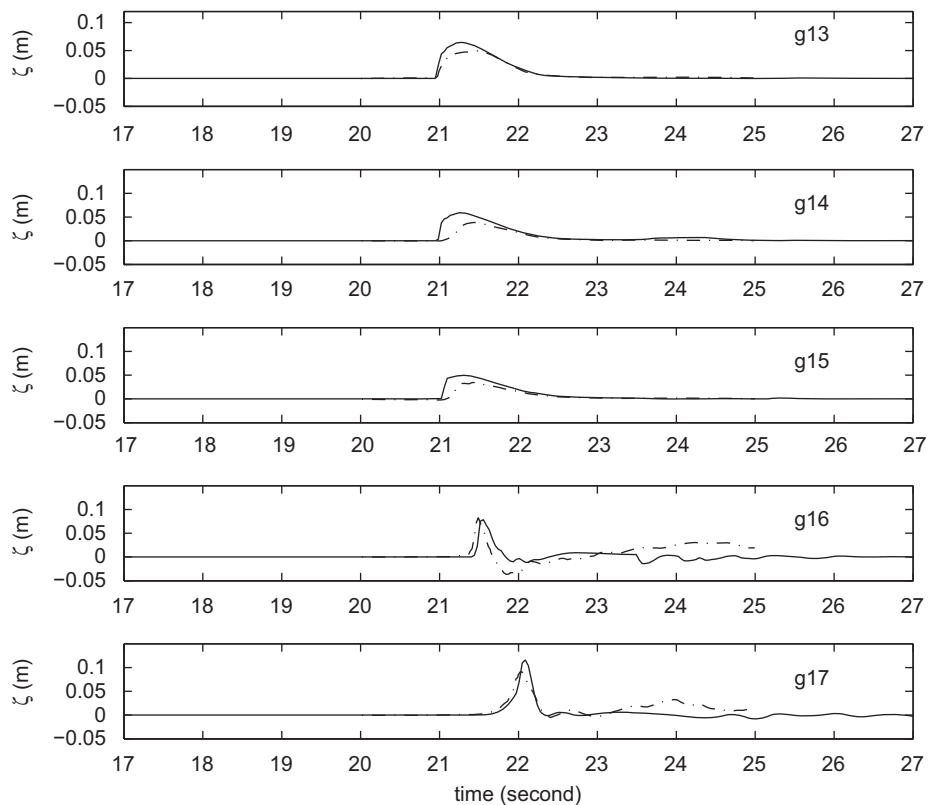


Fig. 14. Time series of the water surface elevations: wave height = 0.12 m, solid: numerical, dotted: experiment. The gage, “g”, locations follow those shown in Fig. 11.

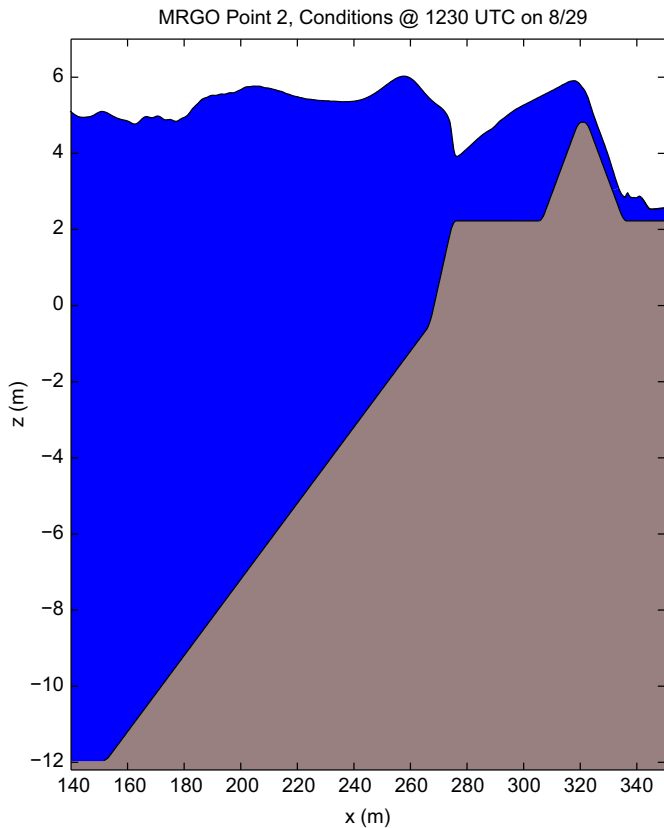


Fig. 15. Simulation snapshot for MRGO point 2 at 1230 UTC, where $H_{mo} = 1.0$ m, surge elevation = 5.3 m, and levee crest elevation = 4.8 m.

computed fluxes are in reasonable agreement with the experimental data and consistent with previously published results.

5.3. Overtopping and backside wave regeneration

HR Wallingford performed a set of experiments on solitary wave overtopping of levees (Dodd, 1998). Here, a simple incident condition, the solitary wave, propagates over a simple trapezoidal levee. Thus from the setup perspective, this might appear as an almost trivial problem. However, with measured time series of water surface elevation in front, over the crest, and along the backside of the levee, we have an ideal numerical benchmark. Such data allows precise comparisons of the predicted physics, uncontaminated by unknown reflections common with wave train studies, and not reliant on experimental means and deviations, which can be predicted with accuracy by a numerical model without said model ever properly capturing the true physics of the problem. If a model can properly recreate the detailed time series of Dodd (1998), it should be expected that the model is robust for overtopping studies, and can be generally applied. It is the approach of this paper that, with proven accuracy for general random wave evolution (e.g. Lynett, 2006), demonstrated accuracy for a standard overtopping benchmark (Saville, 1955), and reasonable agreement for the challenging Dodd data, the presented Boussinesq model can be acceptable for use in the engineering study that comprises the last component of this paper.

The wave flume used in the Dodd (1998) experiments was 40 m long and 0.5 m wide and filled with water to $h_1 = 0.7$ m at the seaward side of the breakwater and $h_2 = 0.3$ m behind the levee. A levee with 1:4 seaward slope and 1:2 leeward slope was

built at the right end of the flume, as shown in Fig. 11. The height of the levee was 0.5 m and the width of the crest was 0.16 m, and it was fronted by a 1:50 inclined floor of height 0.4 m. Five gages were installed on the top of and behind the levee. The first wave gage (13) was located 0.015 m behind the leading edge (A), the second gage (14), and third gage (15) were installed 0.055 and 0.11 m from the first gage, respectively. The fourth gage (16) was located 0.72 m behind the backside edge (B) of the levee. The last gage was installed 0.44 m behind the back toe (C) of the levee as given in Fig. 11. More details of the experimental setup is given in Dodd (1998).

With the wave gages located behind the structure, this dataset provides the rare opportunity to compare not only the overtopping wave, but the regenerated wave behind the structure. Correct simulation of this regenerated wave is considerably more difficult than capturing runup or even overtopping rates. It requires that the model properly simulate the flow down the backface of the structure as well as the reentrance of the overtopping flow into the calm backside water. This latter aspect is the most challenging, and requires a robust and stable method of determining water fluxes in and out of a numerical cell.

Three wave height cases are simulated with the numerical model. The $\Delta x = 0.04$ m, $C_r = 0.5$ and $k_s = 0.0006$ m for plywood are used. The computed profiles of the wave overtopping simulation data are shown in Fig. 12. The left side figures show the profiles when the waves begin overtopping and the right side figures show the small regenerated wave profiles behind the levee. These profiles are verified by the comparison with the laboratory experiment time series data in Figs. 13 and 14. Overall agreement of overtopping with gages 13, 14 and 15 are reasonable. At gages 16 and 17, on the lee side of the levee, the proposed numerical model predicts the dispersive wave motions accurately, which cannot be observed in shallow water equation based model as described in Dodd (1998). There is a clear bias for the numerical model to overpredict the water elevation on the crest, with maximum local errors near the peak on the order of 50%. However, in this area, the model is properly capturing the qualitative shape and arrival time of the wave. Aside from numerical error, this water elevation discrepancy might be due to an incomplete presentation of the initial wave condition, for which there is no provided time series with which to calibrate the incident wave. Overall, the agreement of the Boussinesq model presented here is equal to the Navier–Stokes comparisons of Sitanggang and Lynett (2009) and equal to or better than the shallow water model comparisons of Dodd (1998). With the comparisons presented here, and the established database of literature showing the accuracy of Boussinesq surf zone predictions, it is expected that the model will provide high-confidence nearshore transformation and reasonable overtopping estimates for variable, complex, and steep bathymetry and topography.

6. Simulated overtopping rates along east-facing MRGO levees and correlation with damage observations

6.1. Boussinesq simulation setup

Wave impacts on levees along MRGO are simulated at four specific transects. These four locations correspond to points located within the topographic surveyed levee sections given in Figs. 1–4. The four locations span the length of the east-facing MRGO levees, and represent the range of conditions experienced along the MRGO. The levee profiles are taken from the “Lake Pontchartrain, LA and Vicinity Design Memorandum No. 3” (DM), dated November 1966. Following this DM, the locations examined here are indexed starting from the north, Point 1 (characteristic of

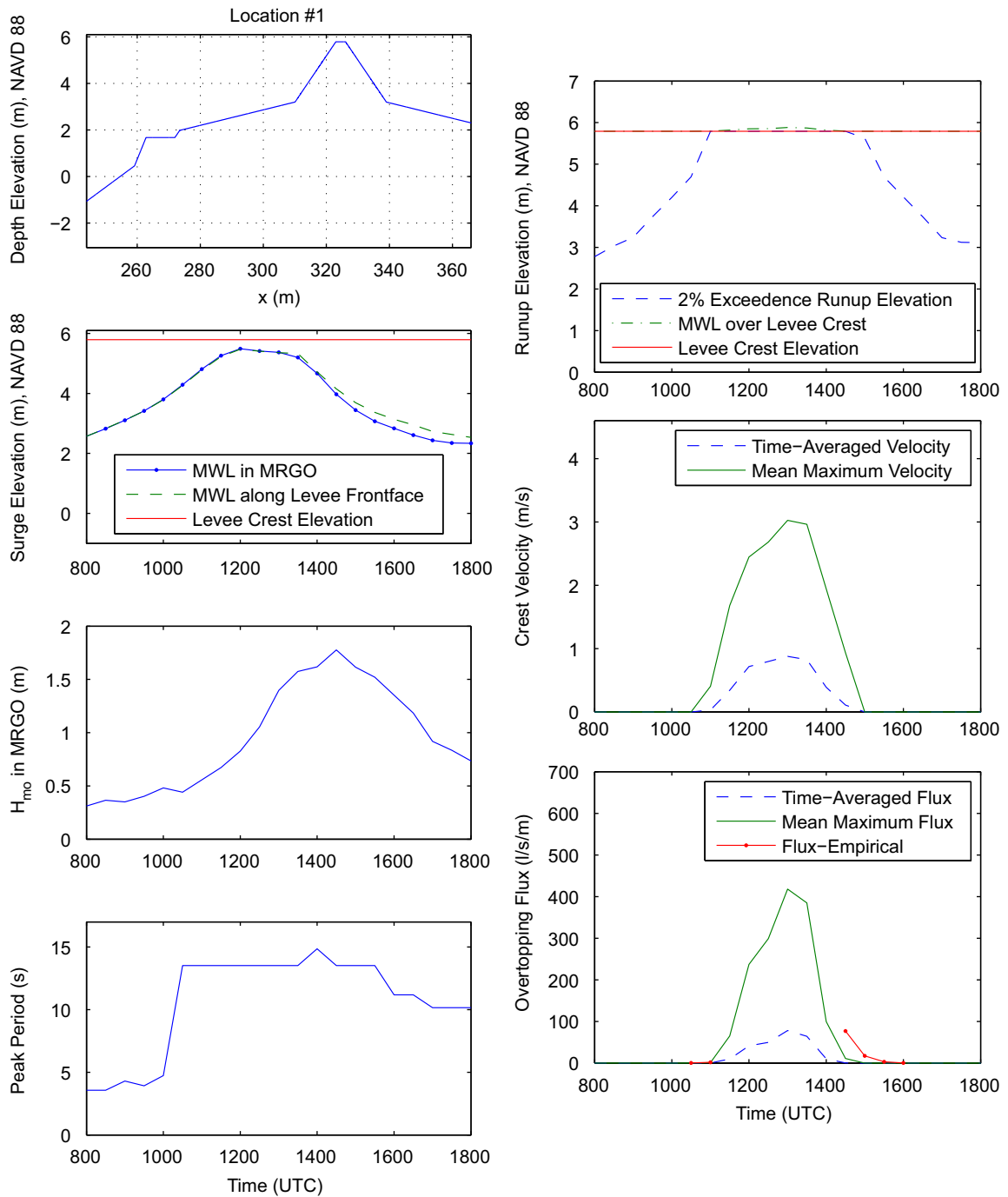


Fig. 16. Boussinesq simulation output summary for MRGO Point 1. The levee cross section is shown in the upper left, and the waves approach the structure from the left. In the lower right (overtopping) subplot, note that the q predicted by the empirical Eqs. (1) and (2), shown by the line with dots, is only plotted for times where the empirical formulation is valid, following Eq. (4). The empirical calculation uses a berm reduction coefficient of 0.9.

levee shown in Fig. 1), Point 2 (characteristic of levee shown in Fig. 2), Point 3 (characteristic of levee shown in Fig. 3), and Point 4 (characteristic of levee shown in Fig. 4). These four locations are also shown with more precision in Fig. 5. The levee profiles from the DM are shifted vertically such that the levee crest elevation matches data from pre-Katrina lidar surveys. Levee crest elevation varies widely along the MRGO, from elevations approaching 5.8 m (NAVD88 2004.65) near at the northern end of the east-facing MRGO levees to values < 4 m in a region of high spatial variability of crest elevation near the Lake Borgne outlet ($x = 8$ km in Fig. 5).

As stated, each of these four levee locations are located near the MRGO channel. This channel is approximately 12 m in depth, with bank side slopes of 1 on 5 to 1 on 10. These bank sides connect to the levee berm, which varies in length, elevation, and profile shape along the length of the MRGO channel. The simulations indicate that waves break sharply as they first reach the berm, in a manner similar to waves hitting a steep shelf or reef. It is this particular characteristic, the short transition from a deep channel to a wide, flat, irregular berm, that makes application of empirical methods challenging. One would need

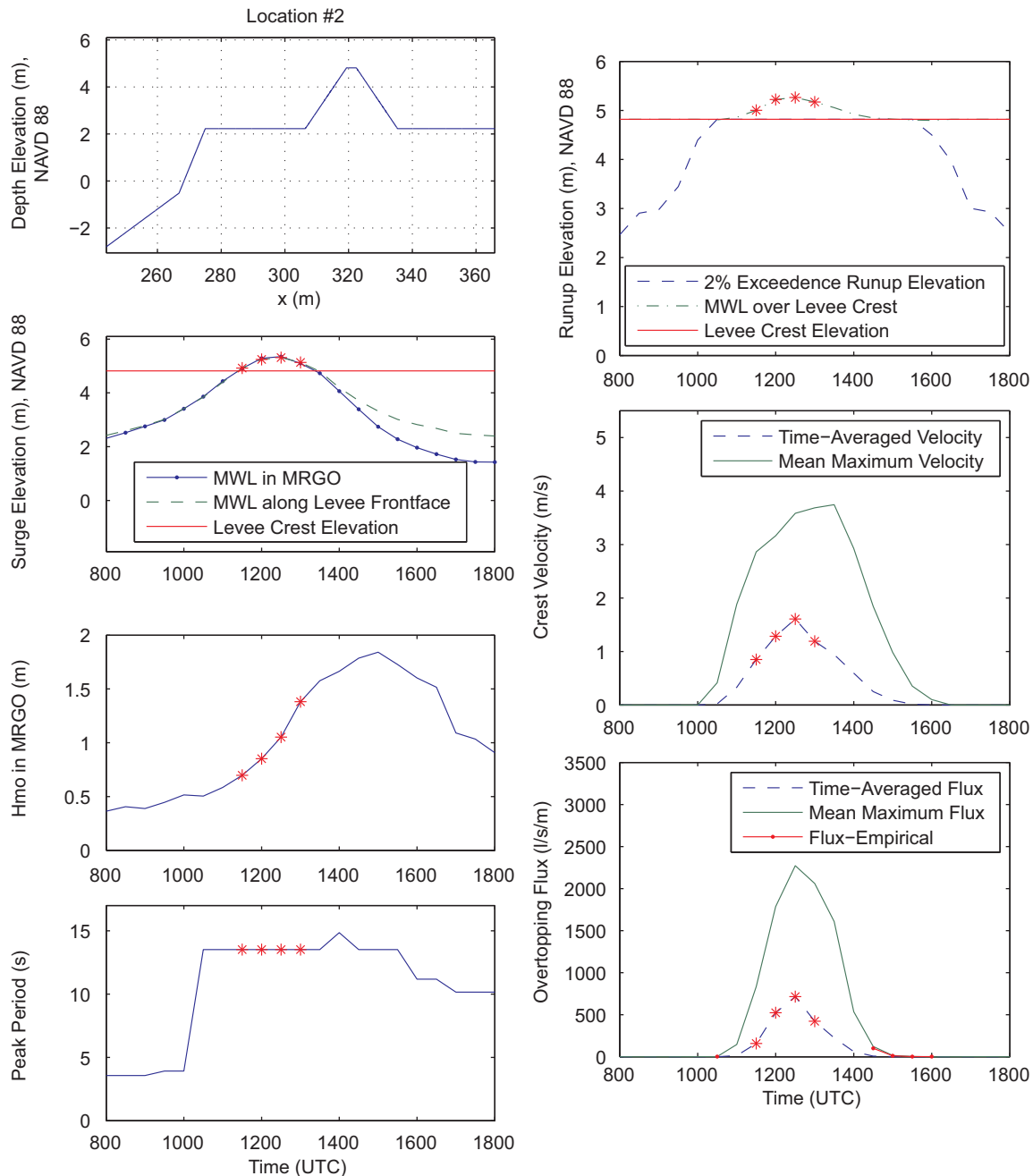


Fig. 17. Boussinesq simulation output summary for MRGO Point 2. The large stars in each of the subplots indicate times when the surge elevation is greater than the levee crest elevation. See the caption for Fig. 16 for other details about the plots.

to specify a berm reduction factor for this unique case, for which there is no established guidance.

Surge and wave conditions are provided by ADCIRC and STWAVE simulations (Interagency Performance Evaluation Team, 2006), recorded just offshore of the levees in the MRGO. Wave and surge conditions are taken at chosen times throughout the storm from 0630 to 1500 UTC on the 29 August 2005, and the quasi-steady conditions at these times are simulated (i.e. for a single simulation, at for example 1230 UTC, the incident wave condition is constant). It is reiterated that the hydrodynamic conditions employed here are from the original IPET study; subsequent studies may provide slightly different conditions. To estimate the worst case hydrodynamics, the 2D spectra provided by STWAVE are reduced to 1D spectra, and the numerical simulations are

performed on a 2D(V) cross-section of the levee. This approach is justified by the observation that the primary wave direction is normal to the MRGO levees, and so predicted 2D(V) hydrodynamics will be a reasonable representation of the full 3D problem. It is noted that while there are little available data to determine the correlation between levee (or seawall) overtopping/runup and peak incident angle for multi-directional spectra, there are indications that the incident angle is not strongly correlated to overtopping rates for incident angles less than 30° , with maximum overtopping occurring at small, but off-normal angles (Owen, 1980). Significant wave heights range of 0.5–1.75 m with peak periods from 4 to 13 s. There is a rapid transition from low periods to high peak periods in the STWAVE data; this is due to the wave spectra becoming abruptly swell dominated.

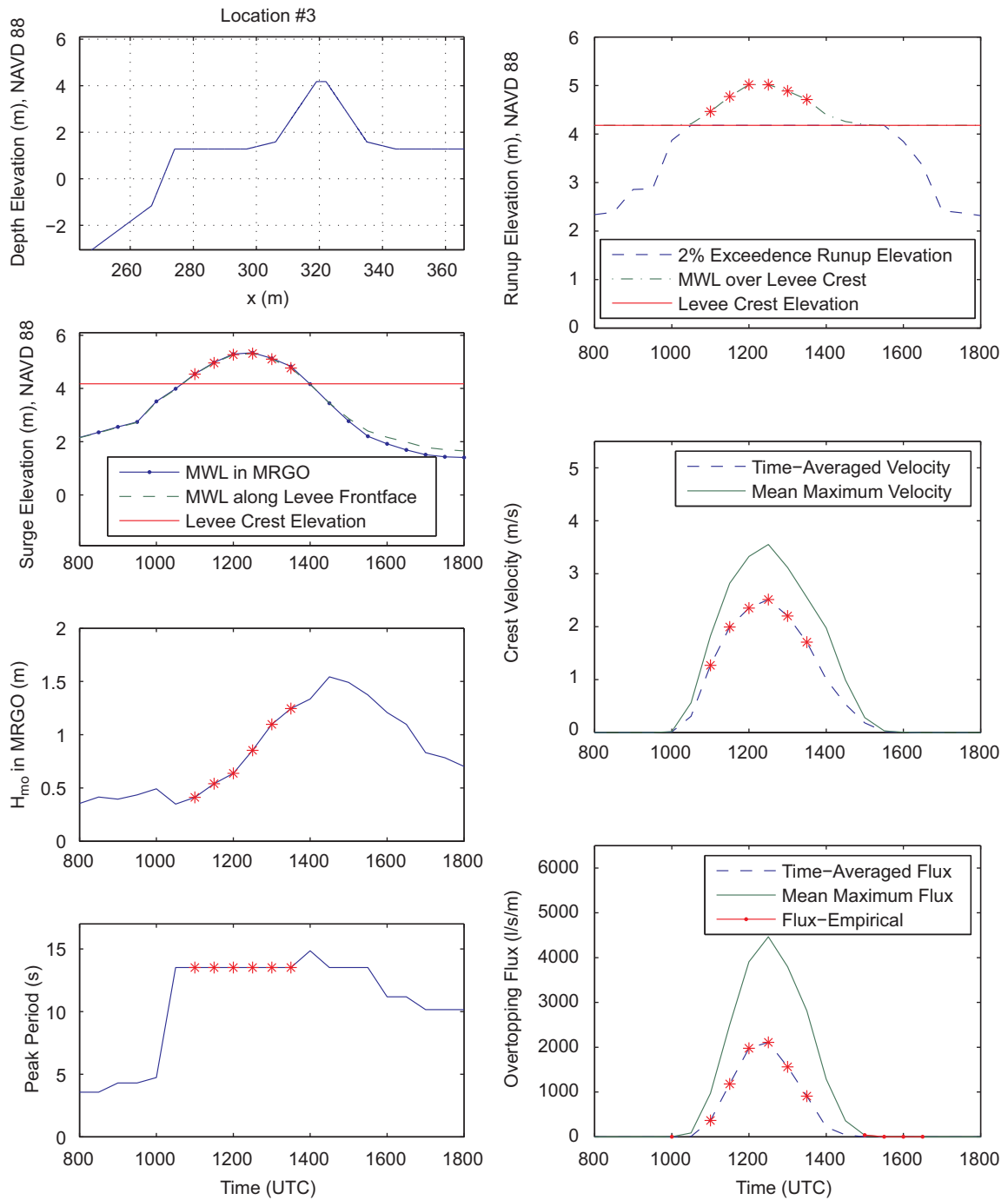


Fig. 18. Boussinesq simulation output summary for MRGO Point 3. The large stars in each of the subplots indicate times when the surge elevation is greater than the levee crest elevation. See the caption for Fig. 16 for other details about the plots.

For each of the four locations, 24 times are simulated, with a range of 0630–1500 UTC, in 30 min increments. The grid resolution used by the simulations is 1 m. Roughness is added to the levee surface to approximate turf; a characteristic bottom roughness height, k_s , of 1 cm is used for all simulations. The simulations provide “instantaneous” information, predicting variations on the order of the time step of the numerical model, approximately $\frac{1}{10}$ of a second. Each simulation is run for 15 min of quasi-steady time. To distill this information for engineering use, time series of free surface elevation, depth-averaged velocity, and volume flux is written at the levee crest. From these time series, time-averaged values and mean maximum values (mean values under the wave crest) are calculated along the levee profile.

6.2. Boussinesq simulation results

An example of the detail provided by these simulations is given in Fig. 15. This figure is a single snapshot (i.e. just one of 30,000 time steps) at location point 2. The physical time corresponding to this condition is 1230 UTC.

A complete summary of the numerical results for the four MRGO locations is provided in Figs. 16–19. The time series of overtopping flux and crest velocity are very closely correlated to the time series of surge. The peak in wave height, occurring 2.5 h after the surge peak leads to a temporal extension of the overtopping, where some of the levees experience overtopping until 1600 UTC. Mean maximum values, due to the wave crest, are 1.5–8 times larger than the

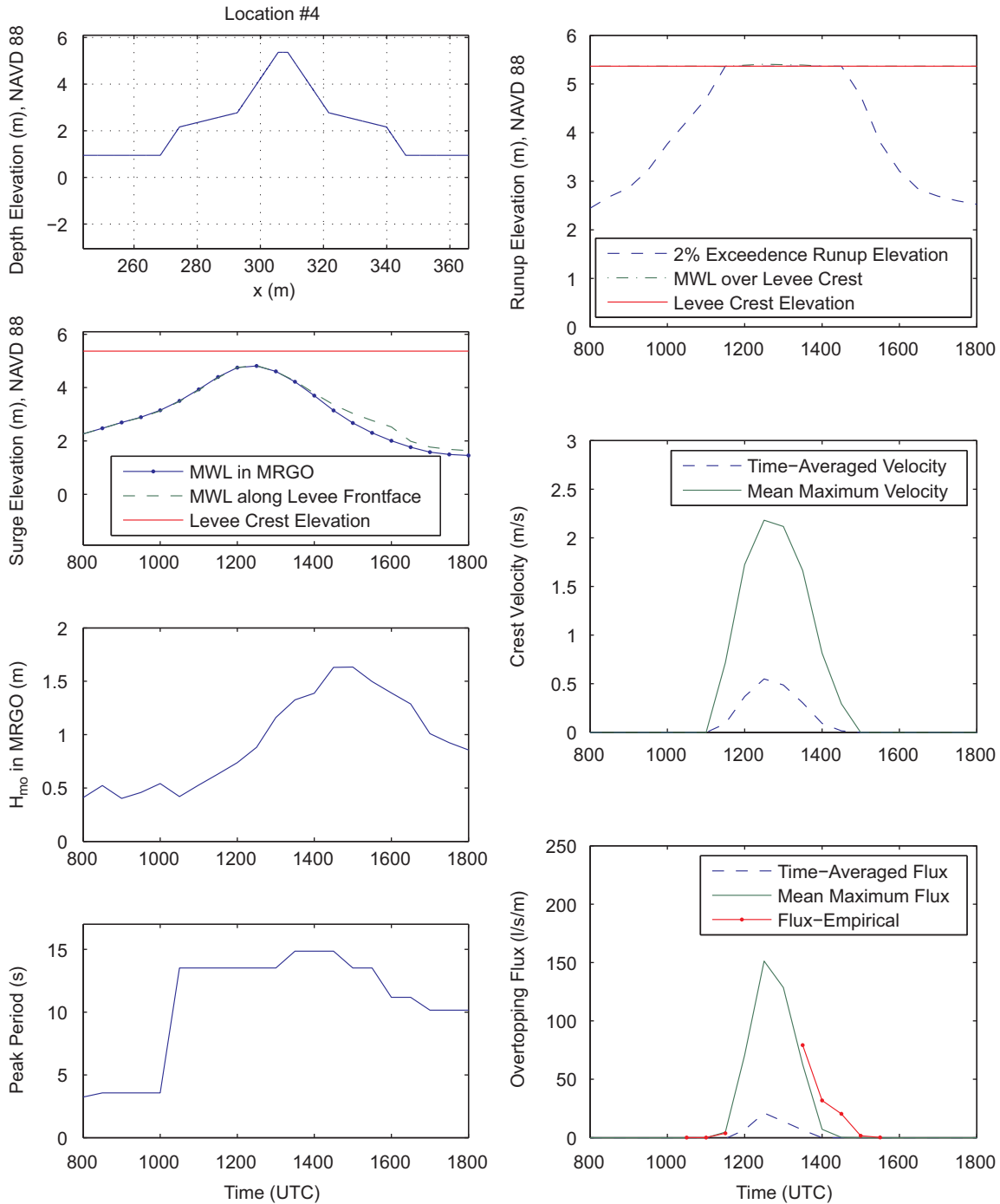


Fig. 19. Boussinesq simulation output summary for MRGO Point 4. See the caption for Fig. 16 for other details about the plots.

time-averaged values. Note that in these figures, in the overtopping subplot (lower right), there is also shown the overtopping prediction based on Eqs. (1) and (2), but these values are only plotted when the validity range, Eq. (4), is satisfied. This validity range is not satisfied during the great majority of the time, due mostly to a small, or negative, freeboard. In addition, the greatest overtopping rates are driven by combined wave and surge; as mentioned there is no established empirical equation for this situation. The empirical overtopping guidance, on its own, is not helpful in estimating the overtopping rates of the MRGO levels during Hurricane Katrina.

For all locations along the length of the MRGO, there is some overtopping from 1130 to 1430 UTC. The maximum overtopping flux takes place between 1230 and 1300, and occurs at the time of

peak surge for all cases. Time-averaged overtopping rates range from 0 to 2000 l/s/m. Values on the low end of this range are due to wave overtopping with a surge less than the levee crest elevation, whereas values on the high end arise from surge elevations 1.2 m above the levee crest, and likely represent the worst conditions experienced along the entire MRGO.

Wave setup does not play a significant role during the peak conditions. This is due to relatively small waves at the time of peak surge (0.6–1.0 m), and the observation that the waves typically initiate breaking just $\frac{1}{4}$ – $\frac{1}{2}$ of a wavelength before overtopping the levee, and thus the wave momentum is carried over the levee, rather than through a dissipative surf zone. Later during the day, near 1500 UTC, the wave height reaches 2 m, and

there is wave setup on the levee front face on the order of 0.3–0.6 m. At this time, however, overtopping is minimal. The levee profile geometry appears to play a strong role in setup. Note that for Location 2 (Fig. 15), the wave setup at 1800 UTC is in excess of 1 m, while the incident wave height is just < 1 m. The reason for this is a surge elevation which is right below the berm elevation. For this particular profile, the berm configuration is flat, similar to a shelf, and water continually piles onto the berm.

6.3. Correlation with Boussinesq-predicted overtopping rate and observed damage

From the Boussinesq-predicted overtopping rates it would be anticipated that locations near point 2 (peak $q = 7501/s/m$) and 3 (peak $q = 22001/s/m$) would have experienced extreme damage, point 1 (peak $q = 801/s/m$) would have experienced moderate damage, and point 4 (peak $q = 101/s/m$) would have experienced negligible to minor damage as the peak overtopping rate does not exceed the 101/s/m threshold for the initiation of erosion. These trends are validated with comparison to the before and after lidar images and data given as Figs. 1–5 which provide the same conclusions.

The benefits, and accuracy, of the Boussinesq model are further exemplified with additional scrutiny of point 4. Again, the simulations show peak overtopping rates near the initiation point of erosion, and the lidar data show only minor scour. On the other hand, the empirical overtopping equations, in the few hours that they are valid, indicate overtopping rates roughly 10 times larger than those predicted by the Boussinesq model. Thus, the empirical guidance suggests that this stretch of levees should have experienced damage at a magnitude that is not consistent with the lidar observations. It is possible, or even likely, that the complex foreshore and bermed cross-section of these levees is beyond the applicability range of the empirical methods. It is noted that the berm reduction coefficient, γ_b , would need to be lowered to a value of 0.35 to yield good agreement with the Boussinesq model predictions. Note that the γ_b in this case would need to take into account the channel bank breaking, which in this case acts similar to a reef break, with strong localized breaking.

7. Integrated overtopping volumes over the MRGO levees

While the Boussinesq simulations already presented do provide insight into the processes that occurred during hurricane Katrina, because there is no lowering of the levee crest elevations due to erosion, they represent a lower limit estimate of the flooding rate. In reality, as the levee crests scoured down, the overtopping volume would have increased. To gage this crest lowering impact, additional analysis is needed.

It is desired to not run many Boussinesq simulations for various crest elevations; this is not an efficient use of the computationally expensive model. Instead, a semi-empirical approach will be employed with the existing Boussinesq model output presented in the previous section. The aim of this analysis will be to provide an estimate of the total overtopping volume along the entire length of the east-facing MRGO levees. To accomplish this, two primary assumptions will be used:

(1) The integrated MRGO overtopping volume will be dominated by the large overtopping rates; wave overtopping with relatively large freeboard can be neglected here.

(2) At a given time, the spatial variation of wave properties along the MRGO is weak, and the overtopping rate can be directly correlated to the freeboard. The wave dependence on the overtopping rate will be hidden within curve-fit coefficients, which will only be applicable to this site for this event.

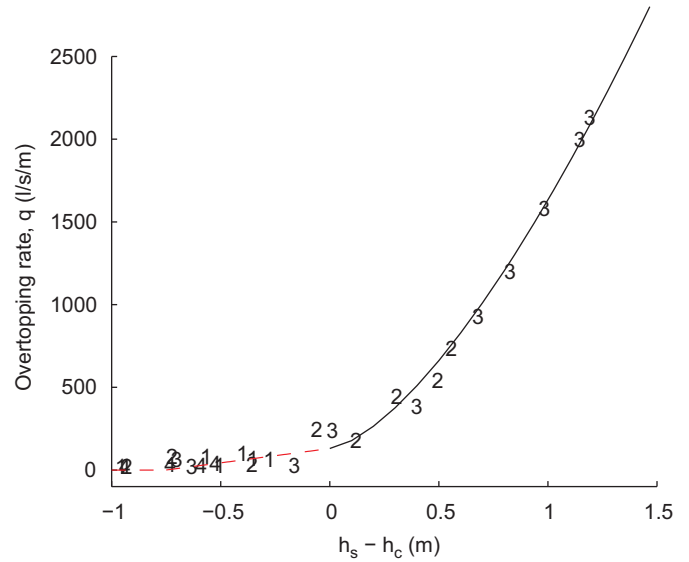


Fig. 20. Overtopping predictions, as a function of surge height minus levee crest elevation, from all Boussinesq simulations. The plotted numbers indicate the MRGO location for each data point, and the dashed curve and the solid curve are given in Eq. (9).

The validity of assumption (2) can be argued through Fig. 20. In this figure, the Boussinesq-predicted overtopping rates from all simulated times are plotted as a function of the negative of the still water freeboard, $h_s - h_c$. In addition to the data points are three curve fit lines, two for a surge level below the crest and a third for the surge level above. These functions are

$$q \approx 0 \quad \text{for } (h_s - h_c) < -0.75 \text{ m}$$

$$q = 0.17(h_c - h_s) + 0.13 \quad \text{for } -0.75 \text{ m} < (h_s - h_c) \leq 0$$

$$q = 0.48\sqrt{g}(h_s - h_c)^{1.5} + 0.13 \quad \text{for } (h_s - h_c) > 0 \tag{9}$$

where q is in $m^3/s/m$ and (h_s, h_c) must be in m. The level of precision and accuracy in the small overtopping curve fit ($h_s - h_c < 0$) is low. Note that this “curve” fit is simply a linear regression through the data. The justification for this minimal effort is taken from assumption 1); these overtopping rates will not contribute significantly to the total volume of water overtopping the MRGO levee system, and so there is not a good reason to press for a better fitting function. Also note that, in this small overtopping region, there is significant relative scatter; the dependence on levee and beach profile geometry and specific wave conditions on wave-driven overtopping is expected. For, $h_c - h_s > 0$, the curve fit equation is taken from steady flow (Eq. (5)), with a slightly smaller leading coefficient and an offset, the 1301/s/m value, which is an average value of the wave overtopping on the MRGO levees when the surge level is equal to the levee crest elevation ($R_c = 0$). The smaller leading coefficient could be due to the bottom roughness effect included in the numerical simulations, or some wave effect. For the case of $R_c = 0$, Eq. (9) yields $q = 1301/s/m$, which would be case-specific for this study only, representing an average zero-freeboard overtopping for the hydrodynamic conditions and cross sections examined here.

Now, with the Boussinesq-based MRGO overtopping Eq. (9) it is possible to estimate the total overtopping rate, Q , integrated spatially along the entire length of the east-facing MRGO levees. Estimates such as these are very useful for drainage and interior hydrology studies. Three different Q 's will be determined: one using the pre-Katrina levee crest elevations, one using the post-Katrina levee elevations, and a third using time-variable crest elevations. The first two estimates provide lower and upper bounds on Q , respectively,

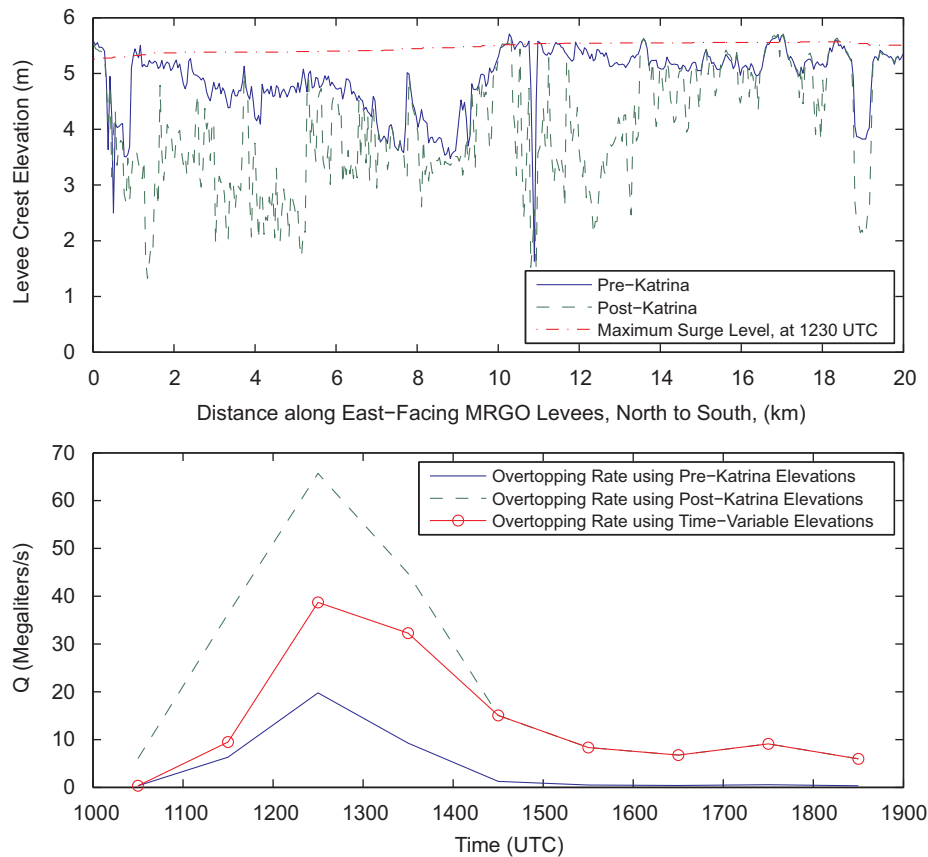


Fig. 21. The top plot shows the before and after Katrina levee crest elevations, with the maximum surge elevation plotted as well. The lower plot gives time series of total overtopping rate, integrated spatially along the entire 20 km of MRGO levees.

while the third is meant to represent a more likely rate. For the time-variable estimate, the levee crest elevations vary linearly from the pre-Katrina elevation at 1030 UTC to the post-Katrina elevation at 1430 UTC. This is a simplification, and does not attempt to correlate the rate of change of levee elevation to the local depth of flow over the crest, as would be physically expected. With the empiricism and approximations already involved here, the additional complexity of a nonlinear change in levee crest elevation is not justified.

Fig. 21 shows the three Q values described in the previous paragraph. The total volumetric rates are tremendously large, and also vary significantly depending on which levee crest elevations are used. Maximum integrated overtopping rates of these MRGO levees likely reached 40 ML/s/m during the peak of the storm.

8. Conclusions

This paper presents a Boussinesq-based approach for estimating the overtopping rates along the east-facing MRGO levees during Hurricane Katrina. For a large fraction of Hurricane Katrina, the wave and surge conditions near the MRGO levees were outside the range of applicability of the established empirical overtopping guidance, and so the Boussinesq model is used as an alternative. The Boussinesq model is used only very near the levees, with waves and water levels provided by STWAVE and ADCIRC simulations performed as part of the IPET effort. In this sense, the modeling approach is multi-scale, as the ADCIRC grid covers the entire Gulf of Mexico, yet the detailed hydrodynamics predicted by the Boussinesq model provides information with a spatial resolution on the order of a meter and temporal resolution of a fraction of a second.

Boussinesq simulations are undertaken at four characteristic transects along the 20 km-long stretch of MRGO levees. These simulations predict overtopping rates consistent with the observed damage; where the levees were eroded heavily the Boussinesq model overtopping estimates are at least an order of magnitude beyond the threshold for levee damage, while at the location that the Boussinesq model predicts a relatively low overtopping rate, minimal scour of the levee crest was found post Katrina.

Finally, the Boussinesq model output was used in a semi-empirical manner to give overtopping rates for all the MRGO levees for the duration of Katrina. These Boussinesq-based overtopping rates provide guidance for combined wave and surge overtopping rates. Interestingly, the combined rate has a very similar form to the steady-flow rate, with a slightly different leading coefficient and an offset equal to the wave-driven overtopping when the still water surge level is equal to the levee crest elevation. In conclusion, we have demonstrated a multi-tiered approach to overtopping estimation; a select few locations were chosen to perform detailed hydrodynamic simulations of wave and surge overtopping, and then these results were used to characterize the entire levee system.

References

- ASCE Hurricane Katrina External Review Panel, 2007. The New Orleans Hurricane Protection System: What Went Wrong and Why. American Society of Civil Engineers, Reston, Virginia, 92pp.
- CEM, Coastal Engineering Manual, 2002. US Army Engineer Research and Development Center, Vicksburg, MS.
- Chen, D., Jirka, G.H., 1995. Experimental study of plane turbulent wakes in a shallow water. Fluid Dynamics Research 16, 11–41.

- De Rouck, J., Verhaeghe, H., Geeraerts, J., 2009. Crest level assessment of coastal structures – General overview. *Coastal Engineering* 56 (2), 99–107.
- Dodd, N., 1998. Numerical model of wave run-up overtopping and regeneration. *ASCE Journal of Waterway, Port, Coastal, and Ocean Engineering* 124, 73–81.
- Haaland, J., 1983. Simple and explicit formulae for the friction factor in turbulent pipe flow. *Journals of Fluids Engineering* 105, 89–90.
- Hu, K., Mingham, C.G., Causon, D.M., 2000. Numerical simulation of wave overtopping of coastal structure using the non-linear shallow water equation. *Coastal Engineering* 41, 433–465.
- Hubbard, M., Dodd, N., 2002. A 2D numerical model of wave run-up and overtopping. *Coastal Engineering* 47, 1–26.
- Hughes, S.A., Nadal, N.C., 2009. Laboratory study of combined wave overtopping and storm surge overflow of a levee. *Coastal Engineering* 56 (3), 244–259.
- Ingram, D.M., Gao, F., Causon, D.M., Mingham, C.G., Troch, P., 2009. Numerical investigations of wave overtopping at coastal structures. *Coastal Engineering* 56 (2), 190–202.
- Interagency Performance Evaluation Team, 2006. Final Report. US Army Engineer Research and Development Center, Vicksburg, MS.
- Kim, D.H., Cho, Y.S., Kim, H.J., 2008. Well balanced scheme between flux and source terms for computation of shallow-water equations over irregular bathymetry. *Journal of Engineering Mechanics* 134, 277–290.
- Kim, D.-H., Lynett, P.J., Socolofsky, S.A., 2009. A depth-integrated model for weakly dispersive, turbulent, and rotational fluid flows. *Ocean Modelling* 27 (3–4), 198–214.
- Kobayashi, N., Wurjanto, A., 1989. Wave overtopping on coastal structures. *ASCE Journal of Waterway, Port, Coastal, and Ocean Engineering* 115, 235–251.
- Li, T., Troch, P., De Rouck, J., 2004. Wave overtopping over a sea dike. *Journal of Computational Physics* 198 (2), 686–726.
- Liu, P.L.-F., Cho, Y.-S., Briggs, M.J., Kanoglu, U., Synolakis, C.E., 1995. Runup of solitary waves on a circular island. *Journal of Fluid Mechanics* 302, 259–285.
- Liu, P., Lin, P.Z., Chang, K.A., Sakakiyama, T., 1999. Numerical modelling of wave interaction with porous structures. *ASCE Journal of Waterway, Port, Coastal, and Ocean Engineering* 125 (6), 322–330.
- Lynett, P., 2006. Nearshore wave modeling with high-order Boussinesq-type equations. *ASCE Journal of Waterway, Port, Coastal, and Ocean Engineering* 132 (5), 348–357.
- Lynett, P., Wu, T.-R., Liu, P.L.-F., 2002. Modeling wave runup with depth-integrated equations. *Coastal Engineering* 46 (2), 89–107.
- Owen, 1980. Design of Seawalls Allowing for Wave Overtopping. Report EX vol. 924, HR Wallingford.
- Powledge, G.R., Ralston, D.C., Miller, P., Chen, Y.H., Clopper, P.E., Temple, D.M., 1989. Mechanics of overflow erosion and embankments II: hydraulics and design considerations. *Journal of Hydraulic Engineering, ASCE* 115 (8), 1056–1075.
- Pullen, T., Allsop, N.W.H., Bruce, T., Kortenhaus, A., Schüttrumpf, H., van der Meer, J.W., 2007. *EurOtop: Wave Overtopping of Sea Defences and Related Structures: Assessment Manual*.
- Reeve, D.E., Soliman, A., Lin, P.Z., 2008. Numerical study of combined overflow and wave overtopping over a smooth impermeable seawall. *Coastal Engineering* 55, p. 155–166.
- Saville, T.J., 1955. Laboratory data on wave run-up and overtopping on shore structures. Tech. Memo No. 64, U.S. Army, Beach Erosion Board, Document Service Center, Dayton, Ohio.
- Schüttrumpf, H., Möller, J., Oumeraci, H., Grüne, J., Weissmann, R., 2001. Effects of natural sea states on wave overtopping of seadikes. In: *Proceedings of the Fourth International Symposium on Waves 2001, Wave Measurement and Analysis, ASCE*, pp. 1565–1574.
- Shao, S., Changming, Ji., David, I.G., Dominic, E.R., Philip, W.J., Andrew, J.C., 2006. Simulation of wave overtopping by an incompressible SPH model. *Coastal Engineering* 53 (9), 723–735.
- Sitanggang, K.I., Lynett, P.J., 2009. Multi-scale simulation with a hybrid Boussinesq-RANS hydrodynamic model. *International Journal for Numerical Methods in Fluids*, DOI: 10.1002/flid.2056.
- Stansby, P., Feng, T., 2004. Surf zone wave overtopping a trapezoidal structure: 1-D modelling and PIV comparison. *Coastal Engineering* 51, 483–500.
- Synolakis, C.E., 1987. The runup of solitary waves. *Journal of Fluid Mechanics* 185, 523–545.
- van der Meer, J., 2002. Technical Report: Wave Runup and Wave Overtopping at Dikes. Technical Advisory Committee on Flood Defence, Delft, The Netherlands.
- Van Ledden, M., Lynett, P., Resio, D., Powell, N., 2007. Probabilistic design method of levee and floodwall heights for the hurricane protection system in the New Orleans area. In: *Proceedings of the 10th International Workshop on Wave Hindcasting and Forecasting, Oahu, Hawaii, USA, November 2007*.
- Yamamoto, S., Daiguji, H., 1993. Higher-order-accurate upwind schemes for solving the compressible euler and Navier–Stokes equations. *Computers and Fluids* 22 (2/3), 259–270.